



Supplement of

Local and transboundary contributions to NO_y loadings across East Asia using CMAQ-ISAM and a GEMS-informed emission inventory during the winter–spring transition

Jincheol Park et al.

Correspondence to: Yunsoo Choi (ychoi6@uh.edu)

The copyright of individual parts of the supplement might differ from the article licence.

Table S1: Modeling setup.

Weather Research and Forecasting (WRF) 3.8.1	
Microphysics	Morrison two-moment scheme (Morrison et al., 2009)
Longwave and shortwave radiation	Rapid Radiative Transfer Model for GCMs (RRTMG) (Clough et al., 2005; Iacono et al., 2008)
Land surface model	Pleim-Xiu land surface model (Xiu and Pleim, 2001)
Surface layer	Pleim-Xiu surface layer (Pleim, 2006)
Planetary boundary layer	ACM2 planetary boundary layer model (Pleim, 2007a; Pleim, 2007b)
Cumulus parameterization	Kain-Fritsch (new Eta) scheme (Kain, 2004)
Four-dimensional data assimilation	FDDA option for grid-nudging (Jeon et al., 2015)
Initial and boundary conditions	National Centers for Environmental Prediction FNL (final) operational model global tropospheric analysis
CMAQ DDM-3D 5.2 and CMAQ-ISAM 5.3.2	
Horizontal advection	YAMO
Vertical advection	WRF omega formula
Horizontal diffusion	Multiscale
Vertical diffusion	ACM2 vertical diffusion scheme (Pleim, 2007a; Pleim, 2007b)
Chemical mechanism	Carbon Bond 5 (cb05tucl) for CMAQ DDM-3D 5.2 Carbon Bond 6 (cb6r3) for CMAQ-ISAM 5.3.2
Aerosol processing module	The 6th generation CMAQ aerosol module (AERO6)
Dry deposition model	M3Dry (Pleim, 2007b)
Boundary condition	Profile (static)

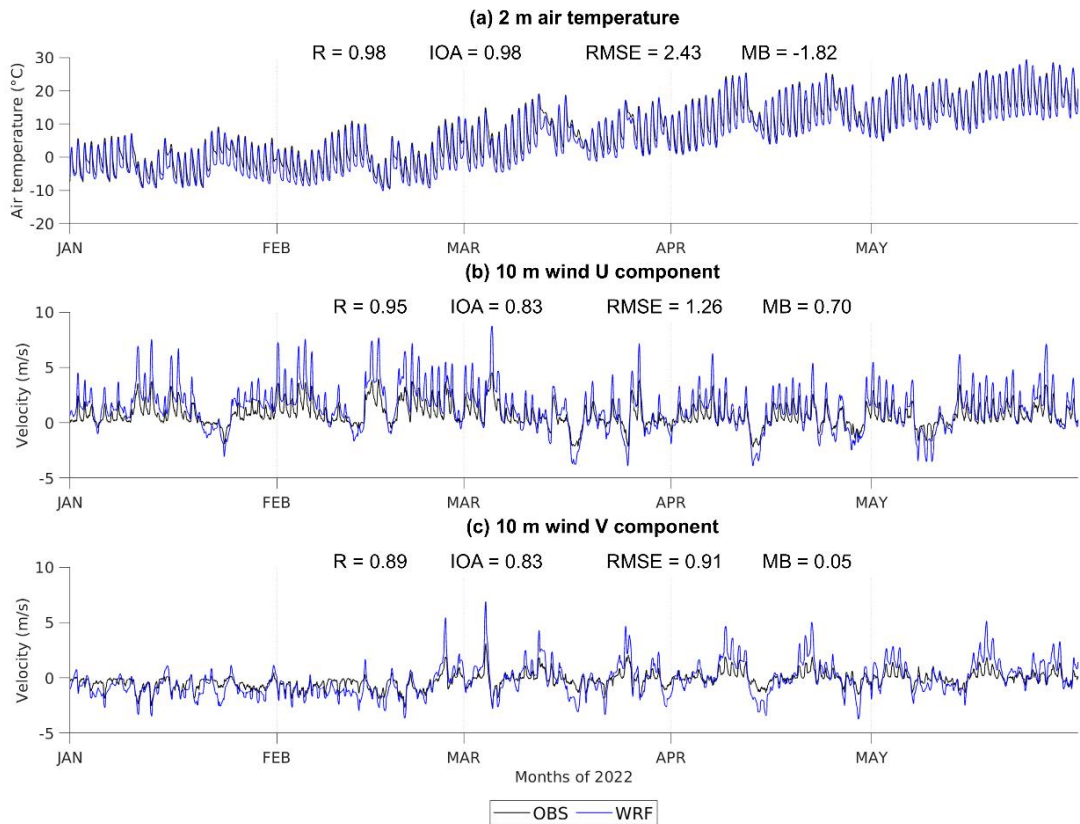
Table S2: Percent changes (%) in inventoried extent of NO_x emissions from the prior to posterior estimates across five regions of East Asia during the period from January to May 2022.

	January	February	March	April	May	Average
South Korea	182.89	41.44	13.13	16.90	-3.79	50.12
Northeast China	29.58	27.44	39.97	33.84	23.45	30.86
North China	55.84	53.76	97.78	98.60	87.19	78.63
East China	14.37	16.74	34.32	27.19	11.20	20.76
South Central China	-7.56	1.07	4.74	13.78	0.98	2.60

Table S3: Descriptive statistics comparing observed and modeled hourly surface PM_{2.5} concentrations averaged at ground-based measurement sites during the period from January to May 2022. Prior: modeled concentrations using the a priori NO_x emissions, Posterior: modeled concentrations using the a posteriori NO_x emissions. R: Pearson's correlation coefficient, IOA: Index of Agreement, NMB: normalized mean bias (%), MAE: mean absolute error (ppb).

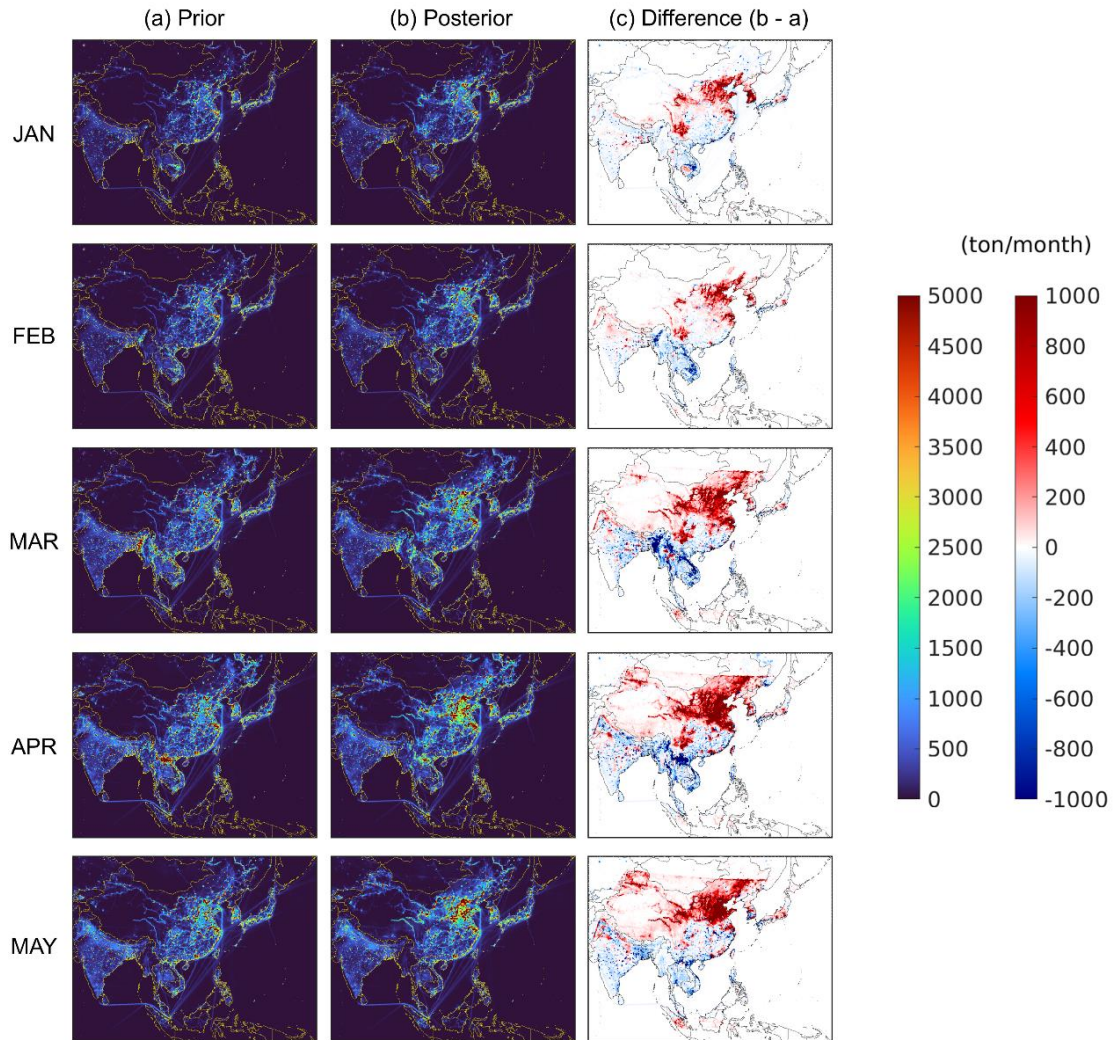
			January	February	March	April	May	5-month
South Korea	Prior	R	0.91	0.92	0.87	0.76	0.77	0.82
		IOA	0.79	0.92	0.90	0.84	0.85	0.86
		NMB	-43.23	-21.55	-15.87	-15.02	-10.47	-21.01
		MAE	11.54	5.66	4.98	4.78	4.20	5.83
	Posterior	R	0.90	0.91	0.86	0.78	0.77	0.82
		IOA	0.80	0.94	0.91	0.86	0.85	0.88
		NMB	-38.21	-14.34	-9.84	-12.37	-10.72	-16.95
		MAE	10.20	5.17	4.68	4.58	4.18	5.44
China	Prior	R	0.53	0.73	0.57	0.51	0.44	0.61
		IOA	0.50	0.66	0.62	0.61	0.65	0.60
		NMB	-49.29	-28.30	-34.16	-32.97	-7.93	-32.50
		MAE	29.52	11.62	15.05	13.65	5.93	14.07
	Posterior	R	0.54	0.75	0.59	0.51	0.45	0.64
		IOA	0.51	0.68	0.63	0.61	0.65	0.62
		NMB	-46.88	-27.79	-31.81	-31.76	-7.85	-31.05
		MAE	28.10	11.34	14.40	13.31	5.83	13.58

Modeled and observed meteorology in Korea



15 **Figure S1:** WRF-simulated hourly surface meteorological fields and those observed at 95 weather stations in South Korea during the period from January 1 to May 31, 2022. (a) 2 m air temperature ($^{\circ}\text{C}$), (b) 10 m wind U component (m/s), and (c) 10 m wind V component (m/s). The black and blue lines indicate the observed and WRF-simulated meteorology, respectively.

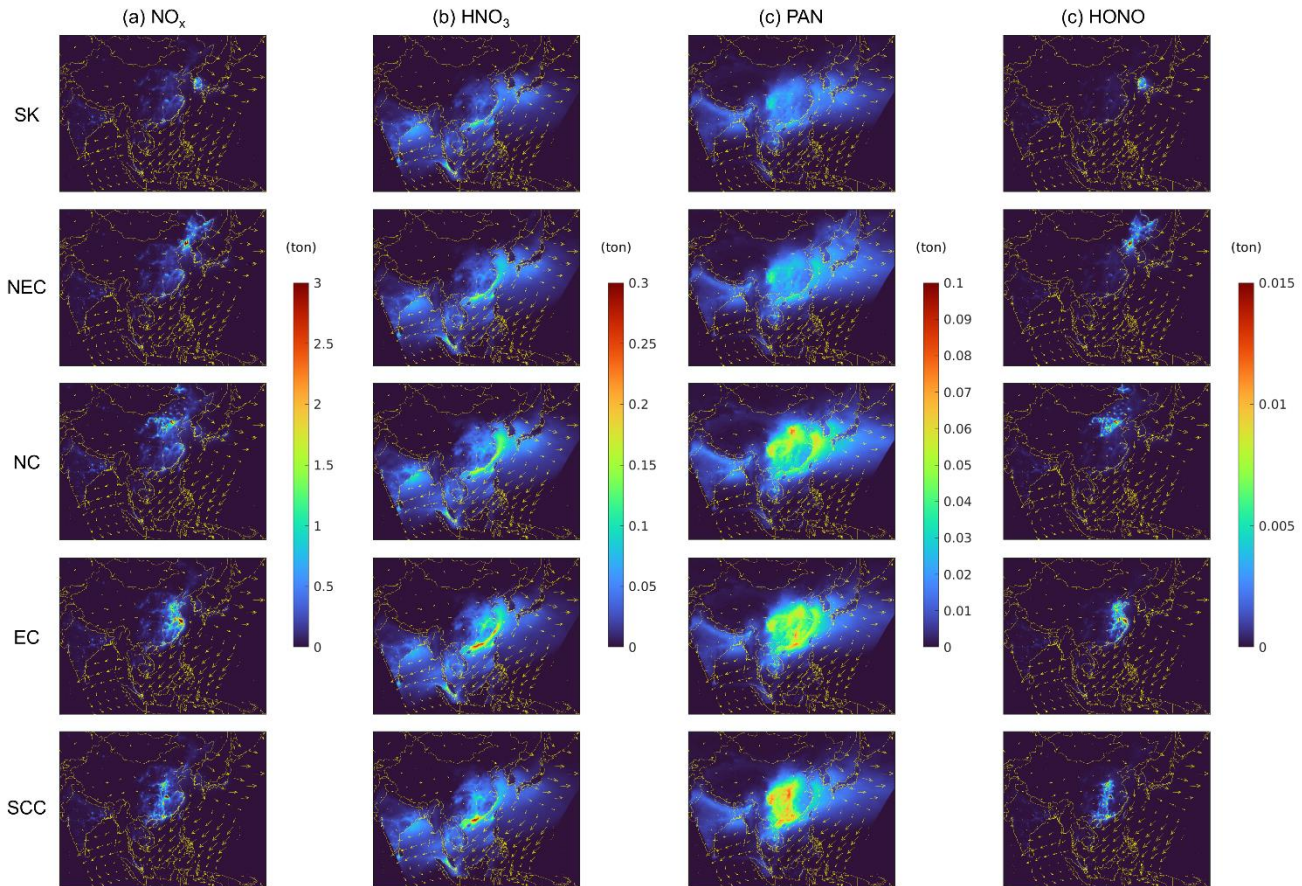
NO_x emissions in Asia



20

Figure S2: Monthly total (sum) NO_x emissions (ton/month) during daylight hours (GEMS retrieval hours) from January to May 2022. (a) the a priori emissions, (b) the a posteriori emissions, (c) differences (b - a).

Source contributions to NO_y components' concentrations across Asia: Winter 2022



25

Figure S3: Source contributions to wintertime total (sum) (a) NO_x, (b) HNO₃, (c) PAN, and (d) HONO concentrations (ton) within the PBL across Asia during the period from January to February 2022. Contributions were quantified based on the simulations using the a posteriori NO_x emissions.

30

Source contributions to NO_y components' concentrations across Asia: Spring 2022

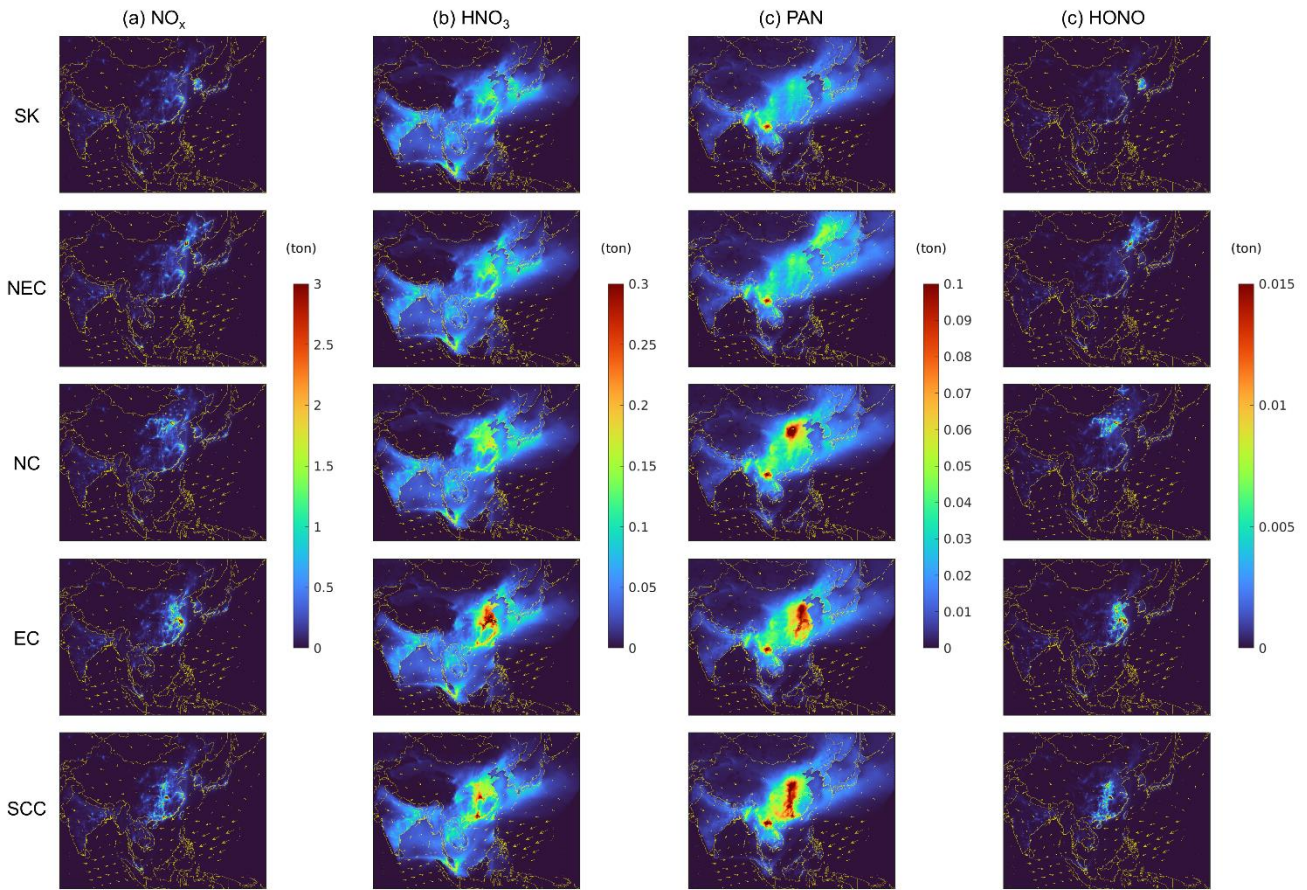


Figure S4: Source contributions to springtime total (sum) (a) NO_x, (b) HNO₃, (c) PAN, and (d) HONO concentrations (ton) within the PBL across Asia during the period from March to May 2022. Contributions were quantified based on the simulations using the a posteriori NO_x emissions.

35

References

- Clough, S. A., Shephard, M. W., Mlawer, E. J., Delamere, J. S., Iacono, M. J., Cady-Pereira, K., Boukabara, S., & Brown, P.
40 D.: Atmospheric radiative transfer modeling: A summary of the AER codes, *J. Quant. Spectrosc. Ra.*, 91(2), 233–244,
<https://doi.org/10.1016/j.jqsrt.2004.05.058>, 2005.
- Iacono, M. J., Delamere, J. S., Mlawer, E. J., Shephard, M. W., Clough, S. A., & Collins, W. D.: Radiative forcing by long-lived greenhouse gases: Calculations with the AER radiative transfer models, *J. Geophys. Res-atmos.*, 113(D13),
<https://doi.org/10.1029/2008JD009944>, 2008.
- 45 Jeon, W., Choi, Y., Lee, H. W., Lee, S.-H., Yoo, J.-W., Park, J., & Lee, H.-J.: A quantitative analysis of grid nudging effect on each process of PM_{2.5} production in the Korean Peninsula, *Atmos. Environ.*, 122, 763–774,
<https://doi.org/10.1016/j.atmosenv.2015.10.050>, 2015.
- Kain, J. S.: The Kain–Fritsch convective parameterization: An update, *J. Appl. Meteorol. Clim.*, 43(1), 170–181,
[https://doi.org/10.1175/1520-0450\(2004\)043<0170:TKCPAU>2.0.CO;2](https://doi.org/10.1175/1520-0450(2004)043<0170:TKCPAU>2.0.CO;2), 2004.
- 50 Morrison, H., Thompson, G., & Tatarskii, V.: Impact of cloud microphysics on the development of trailing stratiform precipitation in a simulated squall line: Comparison of one- and two-moment schemes, *Mon. Weather. Rev.*, 137(3), 991–1007, <https://doi.org/10.1175/2008MWR2556.1>, 2009.
- Pleim, J. E., Xiu, A., Finkelstein, P. L., & Otte, T. L.: A coupled land-surface and dry deposition model and comparison to field measurements of surface heat, moisture, and ozone fluxes, *Water. Air. Soil. Poll.*, 1(5), 243–252.
55 <https://doi.org/10.1023/A:1013123725860>, 2001.
- Pleim, J. E.: A simple, efficient solution of flux–profile relationships in the atmospheric surface layer. *J. Appl. Meteorol. Clim.*, 45(2), 341–347, <https://doi.org/10.1175/JAM2339.1>, 2006.
- Pleim, J. E.: A combined local and nonlocal closure model for the atmospheric boundary layer Part I: Model description and testing, *J. Appl. Meteorol. Clim.*, 46(9), 1383–1395, <https://doi.org/10.1175/JAM2539.1>, 2007a.
- 60 Pleim, J. E.: A combined local and nonlocal closure model for the atmospheric boundary layer Part II: Application and evaluation in a mesoscale meteorological model, *J. Appl. Meteorol. Clim.*, 46(9), 1396–1409,
<https://doi.org/10.1175/JAM2534.1>, 2007b.
- Xiu, A., & Pleim, J. E.: Development of a land surface model Part I: Application in a mesoscale meteorological model, *J. Appl. Meteorol. Clim.*, 40(2), 192–209, [https://doi.org/10.1175/1520-0450\(2001\)040<0192:DOALSM>2.0.CO;2](https://doi.org/10.1175/1520-0450(2001)040<0192:DOALSM>2.0.CO;2), 2001.